PAPER

Check for updates

Enhancing the conversion of ethyl levulinate to γ-valerolactone over Ru/UiO-66 by introducing sulfonic groups into the framework†

Jie Yang, [ID] * Wenjuan Huang, Yongsheng Liu and Tao Zhou

The conversion of ethyl levulinate (EL) to γ-valerolactone (GVL) is an important reaction in biomass conversion. This process undergoes two consecutive reactions: hydrogenation and transesterification of the intermediate compound, *i.e.* ethyl 4-hydroxypentanoate, which are catalyzed by metal nanoparticles and acid sites, respectively. In this study, we explored the catalytic activity of Ru supported on metal organic frameworks aiming to develop efficient metal–acid bifunctional catalysts for this green process. UiO-66 and its analogues with various substituted groups ($-SO_3H$, $-NH_2$ and $-NO_2$) were employed in this study. The Ru particle size, oxidation state and reducibility were characterized by TEM, H_2-TPR, and XPS. The results suggest that the introduction of functional groups reduces the hydrogenation activity of pristine Ru/UiO-66 to various extents. Catalyst modified with $-SO_3H$ group shows much higher acidic catalytic performance while showing hydrogenation activity towards C=O bonds, thus improving the overall transformation of EL to GVL due to the presence of strong Brønsted acid sites.

1 Introduction

Global warming and depletion of fossil resources are two major issues concerning sustainable development.[1] Biomass and its derivatives, as an abundant and inexpensive carbon source for the production of renewable bio-fuels and high value-added compounds, thus attract tremendous attention.[2–5] γ-Valerolactone (GVL), as one of the versatile platform chemicals, can be applied as a fuel additive,[6,7] a green solvent,[8,9] and a precursor of value-added chemicals or liquid hydrocarbon fuels.[8,10] GVL is usually produced by the hydrogenation and successive intramolecular dealcoholization of levulinic acid (LA)[8,11] or its esters.[12,13] Since LA is corrosive and needs formidable purification,[14] employing esters of LA as reactants would be a promising green approach. Taking ethyl levulinate (EL) as an example, two steps are involved in the transformation from EL to GVL:[8,15–17] hydrogenation of EL to ethyl 4-hydroxyvalerate (EHP) and transesterification of EHP to GVL. It is reported that metal catalysts, such as Pd,[18,19] Pt,[19] Ru,[11,19,20] Au,[21] Ni,[22] Co,[23] Mo,[24] and Cu,[25] are all active for hydrogenation of carbonyl groups when hydrogen is used. Among these metal catalysts, Ru has been reported to be the most active component.[14] High catalytic activities of some Ru catalysts in the hydrogenation of LA into GVL have been reported by several research groups.[26–29] For example, Ruppert *et al.*[27] reported a LA conversion of 100%

and a GVL selectivity of 100% in water at 70 °C, 5 MPa over 1 h when employing Ru nanoparticles supported on TiO_2. Recently, Kuwahara *et al.*[28] reported a GVL yield of 95.6% in aqueous medium at 70 °C, 0.5 MPa and 4 h by using Ru nanoparticles confined in Zr-containing spherical mesoporous silica. Galletti *et al.*[30] investigated the catalytic activity of a ruthenium supported catalyst in combination with a heterogeneous acid co-catalyst in the process of hydrogenation of LA to GVL. The result reveals that the presence of the heterogeneous acid co-catalyst is favorable not only for the esterification step, but also for the activation of the carbonyl group, namely hydrogenation to the intermediate γ-hydroxyvaleric acid.

Metal–organic frameworks (MOFs) as a new class of porous crystalline materials are composed by coordination between inorganic metal ions and organic linkers.[30,31] Their tunable structures, physicochemical properties, and functionality[32] make these materials attractive in the applications of catalysis,[33–35] gas storage,[36,37] separation,[38,39] and sensing.[40,41] Zirconium-based MOFs with higher stability in water and some organic solvents[42] have attracted more attention in catalysis.[43–46] Especially, Zr centers act as Lewis and/or Brønsted acid sites under certain reaction conditions, thus being widely applied in many acid-catalyzed reactions.[46–51] UiO-66 ($Zr_6O_4(OH)_4(BDC)_6$ (BDC = 1,4-benezenedicarboxylate)), a perfect crystalline material consisting of $Zr_6O_4(OH)_4$ octahedra featuring a 12-connected Zr_6 cluster with BDC linkers,[52] is an interesting Zr-based MOF due to its multiple acidic property. It is reported that missing linker defect sites always exist in UiO-66 crystals.[53,54] Most likely, in aqueous phase, the defect sites bond with H_2O and $-OH$ groups to compensate the charge lost and

School of Mathematics and Physics, Shanghai University of Electric Power, Shanghai, 200090, China. E-mail: yj_7667@aliyun.com

there are at least three types of Brønsted protons in the UiO-66 framework present on the inorganic nodes: μ_3-OH, $-OH_2$ and $-OH$ protons.[55] Therefore, UiO-66 or organic-functionalized UiO-66 materials can serve as efficient supports with promising acidic catalytic function.

We herein introduced Ru nanoparticles into the frameworks of UiO-66 and its analogues modified with several commonly used functional groups including $-NO_2$, $-NH_2$, and $-SO_3H$, aiming to reveal the effects of the substituted groups on the hydrogenation activity of Ru nanoparticles for the reaction of EL to EHP along with the acid-catalyzed conversion of EHP to GVL *via* transesterification. The results suggest that the Ru/UiO-66–SO_3H catalyst shows the best performance in the overall reaction of converting EL to GVL *via* hydrogenation–transesterification pathways. These findings are helpful for developing efficient bifunctional catalysts for GVL production.

2 Experimental

2.1 Preparation of metal–organic frameworks

According to the literature,[56,57] all of the MOFs were prepared under hydrothermal conditions. For instance, the synthesis of UiO-66–NH_2 was performed by dissolving $ZrCl_4$ (0.30 g) and 2-amino-1,4-benzenedicarboxylic acid (H_2N–H_2BDC) (0.31 g) in DMF (40 mL) at room temperature. The resulting mixture was placed in a Teflon-lined autoclave in a preheated oven at 120 °C for 36 hours. After the solution was cooled to room temperature in air, the resulting solid was filtered and repeatedly washed with absolute ethanol for 3 days while heated at 60 °C in an oil bath. The resulting powder was filtered and dried under vacuum at 50 °C.[57] The functionalized UiO-66s were labelled UiO-66–X (X = $-NO_2$, $-NH_2$, $-SO_3H$).

2.2 Preparation of Ru/UiO-66–X

The supported Ru catalysts were prepared by a wet-impregnation method followed by deposition-reduction of Ru on UiO-66–X. Typically, 0.715 mL of $RuCl_3$ solution (Ru: 21.60 mg mL^{-1}) was impregnated on 0.5 g of UiO-66–X, the resulting sample being labelled $RuCl_3$/UiO-66–X. After drying at 60 °C, $RuCl_3$/UiO-66–X was immersed into 60 mL of methanol with stirring. The Ru precursor was reduced with $NaBH_4$ methanol solution. The solid was filtered and dried at 50 °C under vacuum. The resulting products were denoted as Ru/UiO-66–X.

2.3 Characterization

Powder X-ray diffraction (XRD) patterns were collected with a Rigaku Ultima IV X-ray diffractometer using Cu Kα radiation (λ = 1.5405 Å) operated at 35 kV and 25 mA. Scanning electron microscopy (SEM) was performed with a Hitachi S-4800 at 10 kV. Transmission electron microscopy (TEM) images were obtained with a FEI Tecnai G^2 F30 microscope operated at 300 kV. Fourier transform infrared (IR) spectra were collected with a Nicolet Fourier transform infrared spectrometer (NEXUS 670). Liquid nitrogen adsorption was used to determine the BET surface areas and pore volumes. Prior to the adsorption

measurements, the samples were degassed *in situ* under vacuum at 150 °C for 6 h. Inductively coupled plasma (ICP) analysis was used to quantify the Ru loading with a Thermo IRIS Intrepid II XSP atomic emission spectrometer. Samples were firstly dissolved in *aqua regia* and then diluted with deionized water. X-ray photoelectron spectroscopy (XPS) was conducted with an ESCALAB 250xi spectrometer, using a monochromated Al Kα X-ray source ($h\nu$ = 1486.6 eV). High-resolution spectra were obtained using 40 eV pass energy and 0.1 eV step. Instrument base pressure was 8×10^{-10} Pa. All binding energies were referenced to the C 1s line at 284.6 eV. Due to the strong overlap between Ru 3d with C 1s, the Ru $3d_{5/2}$ peaks were analyzed. Before each measurement, the samples were pretreated by reducing in a hydrogen atmosphere at a reaction temperature (80 °C), stored in isopropanol and then transferred onto the sample holder in a glove box. To investigate the adsorption behavior of EL on supports, thermogravimetric analysis was performed with a NETZSCH STA449F3 TGA. Samples were heated from room temperature to 800 °C with a heating rate of 10 °C min^{-1} under an air flow. Temperature-programmed reduction (TPR) measurements were carried out using a TP-5080 (Tianjin Xianquan, China) equipped with a thermal conductivity detector. Prior to measurements, about 50 mg of sample was pretreated in a He stream, heated to 150 °C at a rate of 10 °C min^{-1}, and held at this temperature for 1 h. After cooling down to room temperature, a gaseous mixture of 5% H_2 in Ar was fed at a flow rate of about 30 mL min^{-1} and the sample was heated to 150 °C with a rate of 10 °C min^{-1}.

2.4 Catalytic activity measurements

The hydrogenation of EL in water was carried out in a Teflon-lined (120 mL) steel batch reactor. As-prepared catalysts were loaded into the reactor with 9.6 mL of deionized water and 340 µL of EL. After purging five times with H_2, the reactor was pressurized with 0.5 MPa H_2 and the rector was placed in an oil bath which was kept at 80 °C and the liquid was vigorously stirred to reduce the mass transfer effect. The transesterification of EHP in water was carried out in a glass pressure bottle. As-prepared catalysts were loaded into the bottle charged with 5 mL of deionized water and 200 µL of a mixture of EHP (84 mol%), GVL (5 mol%), and EL (11 mol%). The bottle was placed in an oil bath at 80 °C with stirring for 8 hours. All of the products were diluted with ethanol and analyzed with a Tian-mei 7900 GC equipped with a DM-FFAP capillary column (30 m length, 0.25 µL film thickness and 0.25 mm internal diameter).

3 Results and discussion

3.1 XRD, IR and BET characterization of UiO-66 and UiO-66–X

Fig. 1A displays the XRD patterns of the series of isostructural UiO-66. According to the XRD results, all materials show similar structure well matching the patterns in the literature.[56,57] To confirm the successful incorporation of various substituents, *i.e.* $-SO_3H$, $-NH_2$ and $-NO_2$, the IR spectra of UiO-66, UiO-66–NH_2, UiO-66–SO_3H and UiO-66–NO_2 were compared as shown
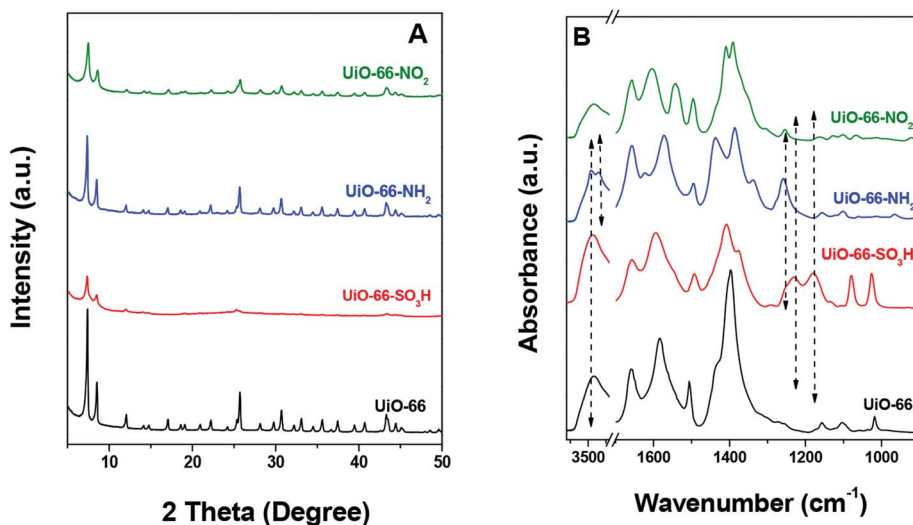
Fig. 1 (A) XRD patterns of UiO-66 and UiO-66–X and (B) IR spectra of UiO-66 and UiO-66–X.

in Fig. 1B. In the case of UiO-66–SO_3H, the bands at *ca.* 1080 and 1180 cm^{-1} are assigned to the stretching modes of –SO_3H with double-bond character (O=S=O).[44] The band at *ca.* 1025 cm^{-1} is due to the stretching vibration of the S–O single bond.[44] The presence of –NH_2 is confirmed by the presence of the bands at 3458 and 3353 cm^{-1} due to the N–H vibration,[44] as well as the C–N stretching band at 1257 cm^{-1}.[57,58] The peak at 1540 cm^{-1}, attributed to the asymmetric –NO_2 stretching vibration, proves the existence of nitro groups in UiO-66–NO_2.[44] N_2 physisorption was used to determine the BET surface areas (Fig. S1†) and the results are listed in Table 1. UiO-66 has a specific surface area (SSA) of 575 $m^2 g^{-1}$. The SSAs of UiO-66–NH_2 and UiO-66–NO_2 are 661 and 651 $m^2 g^{-1}$, respectively, which are ~13% higher than that of UiO-66. In contrast, the SSA of UiO-66–SO_3H (284 $m^2 g^{-1}$) is much lower than that of UiO-66, which is likely due to steric constraints and increased molecular weight resulting from the 2-substituted sulfonic group.[56,57] A promising approach to achieve modulation of the physical properties of UiO-66–SO_3H is to combine different ligands of the same denticity in different proportions, namely 1,4-benzenecarboxylic acid and 2-substituted 1,4-benzenecarboxylic acid.[56] We cannot exactly determine the pore size distribution by N_2 adsorption at this stage due to the microporous nature. The particle sizes of these materials range from 200 to 600 nm according to the SEM images (Fig. S2†).

3.2 Characterization of Ru/UiO-66 and Ru/UiO-66–X

Fig. 2 shows the XRD patterns of UiO-66 and UiO-66–X after loading with Ru nanoparticles. All Ru/UiO-66–X materials retained their crystalline structures, except for Ru/UiO-66–SO_3H. The long-range order of Ru/UiO-66–SO_3H collapsed after $RuCl_3$ impregnation and reduction, indicating its unstable structure as reported in the literature.[56] No diffraction peaks attributed to Ru nanoparticles were observed in the XRD patterns of Ru/UiO-66 and Ru/UiO-66–X, indicating the high dispersion of the Ru particles. N_2 physisorption results of Ru/

Table 1 Physicochemical properties of UiO-66 and Ru/UiO-66–X

Catalyst	SSA ($m^2 g^{-1}$)	Ru^a (wt%)	H/Ru^b
UiO-66	575	—	—
UiO-66–SO_3H	284	—	—
UiO-66–NH_2	661	—	—
UiO-66–NO_2	651	—	—
Ru/UiO-66	510	2.3	0.89
Ru/UiO-66–SO_3H	10	1.7	0.64
Ru/UiO-66–NH_2	170	4.0	0.16
Ru/UiO-66–NO_2	489	1.7	0.47

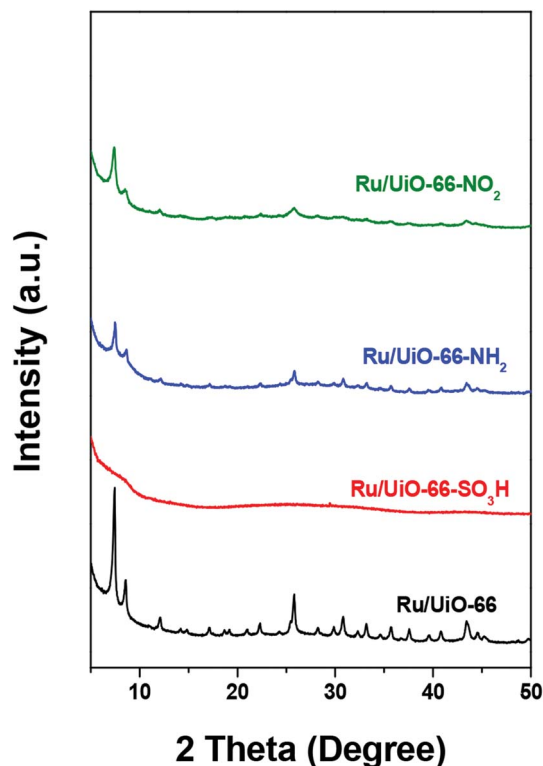*a* Determined by ICP-AES. *b* Calculated from H_2-TPR results.

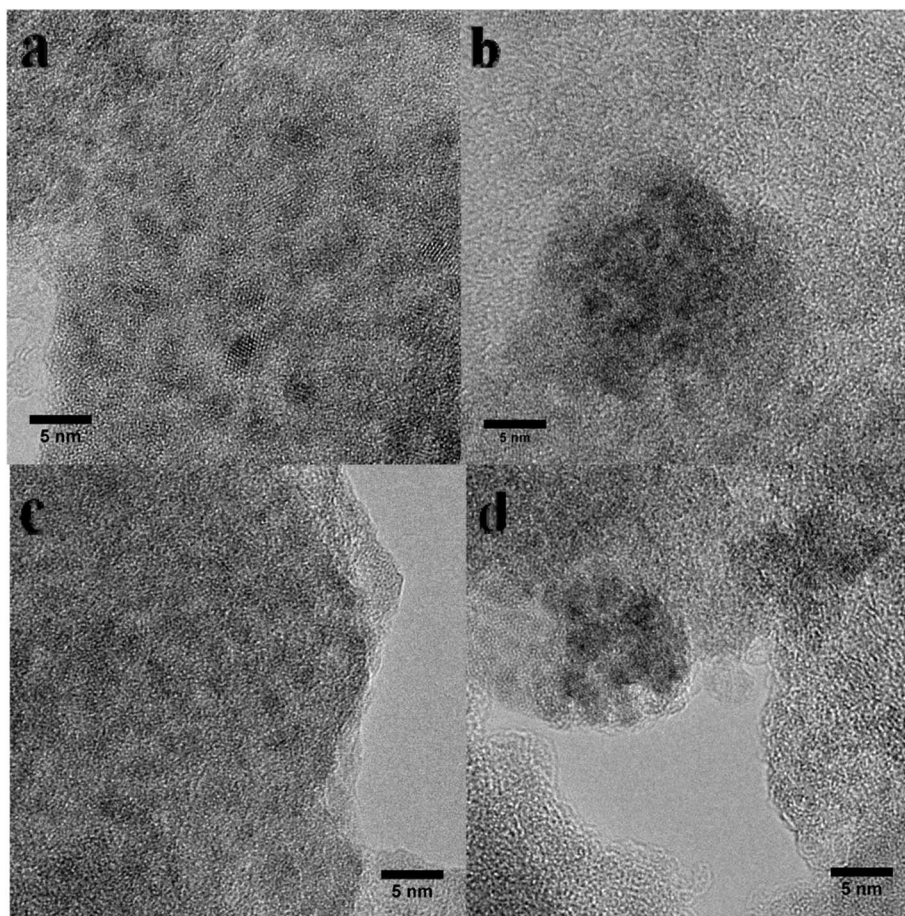**Fig. 2** XRD patterns of Ru/UiO-66 and Ru/UiO-66–X.

Fig. 3 TEM images of (a) Ru/UiO-66, (b) Ru/UiO-66–SO₃H, (c) Ru/UiO-66–NH₂ and (d) Ru/UiO-66–NO₂.

UiO-66 and Ru/UiO-66–X (Table 1 and Fig. S3†) reveal that the SSA of UiO-66 is retained after loading Ru nanoparticles. The SSA of Ru/UiO-66–NO₂ is 489 m² g⁻¹, which is lower than that of the pristine material. However, after Ru loading, the SSAs of UiO-66–SO₃H and UiO-66–NH₂ dramatically decrease by 96% and 74% compared with the pristine materials, which could be explained by the compromised structures of UiO-66–SO₃H and UiO-66–NH₂ upon Ru loading.

The Ru loadings were determined by ICP analysis and the results are listed in Table 1. The Ru loading is close to 2 wt% for the catalysts except for Ru/UiO-66–NH₂. Ru loading of Ru/UiO-66–NH₂ is about 4 wt% which is higher than that of the other Ru/UiO-66–X. This result suggests that the incorporation of Ru species is successful for Ru/UiO-66–NH₂, which may be due to a strong coordination ability of –NH₂ group with Ru species, leading to the high loading efficiency. The particle sizes of Ru for Ru/UiO-66–X were analyzed by high-resolution TEM (Fig. 3), the Ru particle sizes of all catalysts being in the range of 1–4 nm. It should be noted that the Ru particles of UiO-66–NH₂ are smaller than those of the other catalysts.

The H₂-TPR profiles of all catalysts are shown in Fig. 4. A significant H₂ consumption peak ranging from 40 to 120 °C was observed for all catalysts, which is attributed to the reduction of oxidic Ru species below 150 °C.[59] This result is consistent with
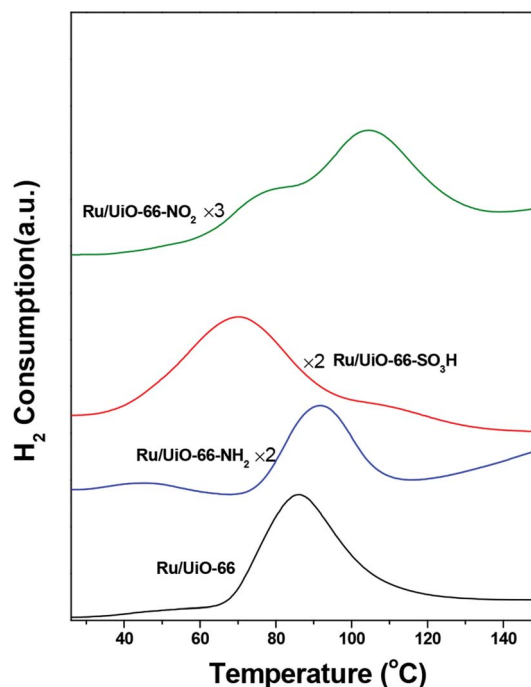

Fig. 4 H₂-TPR profiles of fresh Ru/UiO-66, Ru/UiO-66–NH₂, Ru/UiO-66–SO₃H and Ru/UiO-66–NO₂.
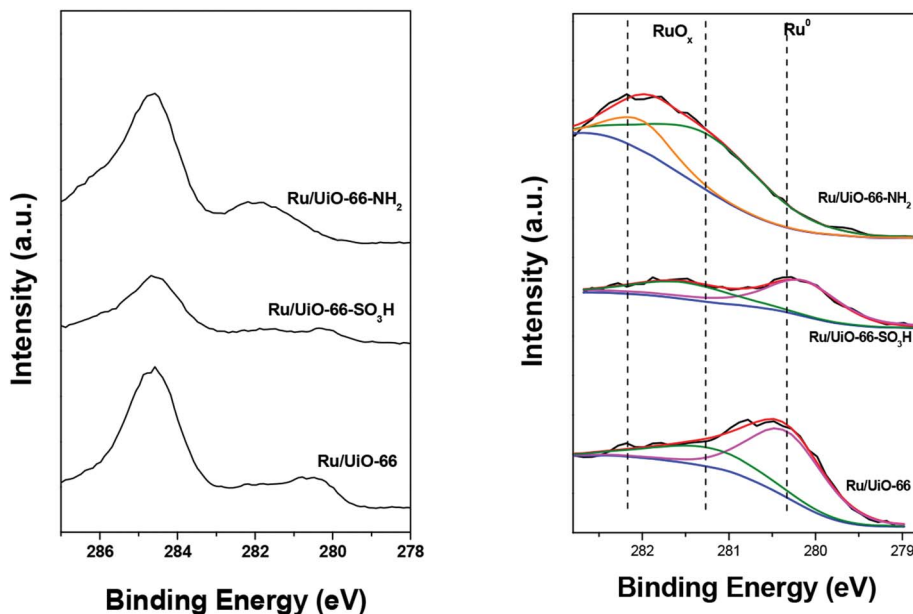
Fig. 5 XPS spectra of Ru 3d C^{-1} 1s region of Ru/UiO-66, Ru/UiO-66–NH$_2$ and Ru/UiO-66–SO$_3$H (left) and fitted XPS spectra of Ru 3d$_{5/2}$ region of Ru/UiO-66, Ru/UiO-66–NH$_2$ and Ru/UiO-66–SO$_3$H (right). The dashed lines indicate the binding energies of the 3d$_{5/2}$ peaks of reduced Ru (Ru^0, magenta asymmetric curves) and oxidic Ru (green symmetric curves and orange symmetric curves) species. Red lines represent the overall fit of the data and blue lines represent background.

the fact that Ru particles are prone to being oxidized when exposed to oxygen. We have roughly calculated the H/Ru ratio by normalizing on the amount of Ru loading. The H/Ru ratios of Ru/UiO-66, Ru/UiO-66–SO$_3$H, Ru/UiO-66–NH$_2$ and Ru/UiO-66–NO$_2$ were found to be 0.89, 0.64, 0.16 and 0.47, respectively. One finding is that UiO-66–NH$_2$ shows much lower H$_2$ consumption compared with the other samples, which results from the stronger interaction between –NH$_2$ and oxidic Ru species. In addition, the reduction of oxidic Ru takes place at 65 °C for Ru/UiO-66. The introduction of –SO$_3$H group leads to a lower reduction temperature starting at 40 °C, while introducing –NO$_2$ and –NH$_2$ groups both leads to higher reduction temperature starting at about 80 °C. The result suggests that the reducibility of oxidic Ru species supported on UiO-66 is dependent on the organic groups introduced. The –SO$_3$H functional group benefits the reduction of Ru species at lower temperatures, which plays a critical role in the hydrogenation process under mild conditions because metallic Ru species generally show better hydrogenation activity towards C=O group than their oxidized counterparts.[59]

We also investigated the reduction degree of the supported Ru particles upon pretreatment under a H$_2$ flow at 80 °C for 30 min by XPS. The fitted Ru 3d XPS spectra of the Ru/UiO-66

sample series and the corresponding results are shown in Fig. 5 and Table 2. Ru (3d) peaks are resolved as a doublet (3d$_{5/2}$ and 3d$_{3/2}$ at 279.90 and 284.07 eV, respectively) with an SOS of 4.17 eV.[60] Because the 3d$_{3/2}$ peak centered at *ca.* 284 eV is always overlapped by the C 1s peak, we herein focused on the Ru 3d$_{5/2}$ peak which can be generally deconvoluted into three oxidation states: the feature at *ca.* 280 eV can be ascribed to metallic Ru, whereas the peaks at *ca.* 281 and 282 eV are ascribed to RuO$_2$. In the cases of UiO-66 and UiO-66–SO$_3$H, the peaks of Ru^0 were clearly observed at about 280.2 eV upon flushing with H$_2$ at 80 °C. It has been previously shown that the oxidized Ru particles on UiO-66 can be partially reduced by H$_2$ at room temperature.[59] The contents of metallic Ru on UiO-66 and UiO-66–SO$_3$H were calculated to be *ca.* 71% and 60%, respectively. This result implies that both oxidic RuO$_x$ and metallic Ru are present in Ru/UiO-66 and UiO-66–SO$_3$H at 80 °C in H$_2$ atmosphere and the metallic Ru is present dominantly. For Ru/UiO-66–NH$_2$, we only observed RuO$_2$ from XPS, meaning that the Ru$^{\delta+}$ cations are strongly coordinated to –NH$_2$ groups. Similar results have been previously reported by Wang *et al.* for a ruthenium-supported catalyst containing –NH$_2$ groups.[61] These results indicate that the functional groups on the ligands play a prominent role in the redox behavior of Ru species.

Table 2 Binding energies (BE) and calculated reduction degree (RD) of the fitted Ru 3d$_{5/2}$ XPS spectra of Ru/UiO-66, Ru/UiO-66–SO$_3$H and Ru/UiO-66–NH$_2$

Sample	Ru^0 3d$_{5/2}$ BE (eV)	Ru^{3+} 3d$_{5/2}$ BE (eV)	Ru^{4+} 3d$_{5/2}$ BE (eV)	RD (3d$_{5/2}$, %)
Ru/UiO-66	280.3	—	281.2	71
Ru/UiO-66–SO$_3$H	280.1	—	281.5	60
Ru/UiO-66–NH$_2$	—	282.0	281.2	0

3.3 Catalytic activity measurements

The activities of Ru/UiO-66 and the three modified Ru/UiO-66 materials in the hydrogenation of EL were tested by using each catalyst of 100 mg in water at 80 °C for 1 h under 0.5 MPa of H$_2$. The conversion of EL and selectivity of GVL and EHP after reaction for 1 h are listed in Table 3. It is clear that Ru/UiO-66 shows the highest hydrogenation activity with EL conversion of 100%. The conversions of EL on Ru/UiO-66–SO$_3$H, Ru/UiO-66–NO$_2$ and Ru/UiO-66–NH$_2$ are 95, 82 and 37%, respectively. These results suggest that the introduction of functional groups reduces the hydrogenation activity of supported Ru nanoparticles to different extents. –SO$_3$H groups do not reduce the hydrogenation activity markedly; whereas –NH$_2$ groups may strongly coordinate with Ru surface sites thus hampering the activation of H$_2$ and the adsorption of EL. The selectivity of GVL when using Ru/UiO-66, Ru/UiO-66–SO$_3$H, Ru/UiO-66–NO$_2$ and Ru/UiO-66–NH$_2$ is 50, 61, 40 and 29%, respectively. UiO-66–SO$_3$H containing strong Brønsted acidity shows the highest GVL selectivity. These results emphasize the importance of Brønsted acidity in transesterification reaction and prove the positive role of –SO$_3$H in the transesterification of EHP. Prolonging the reaction period to 5 h leads to a full conversion of EL and 100% selectivity to GVL (Table S1†) on Ru/UiO-66 and Ru/UiO-66–SO$_3$H. The above results reveal that introducing –SO$_3$H groups does not reduce the activity of Ru/UiO-66 in the hydrogenation of EL, while enhancing the transesterification step, leading to higher activity in converting EL to GVL.

To shed further light on the promotion effect of –SO$_3$H groups on the overall reaction, the reactivities on Ru/UiO-66, Ru/UiO-66–NO$_2$ and Ru/UiO-66–SO$_3$H were studied in detail by employing varying amounts of the catalysts in water at 80 °C for 1 h under 0.5 MPa of H$_2$. The results are listed in Table 3. 25 mg of the catalysts gave EL conversions of 98%, 11% and 29% for Ru/UiO-66, Ru/UiO-66–NO$_2$ and Ru/UiO-66–SO$_3$H, respectively. By increasing the amount of the catalysts to 50 mg, EL conversion on Ru/UiO-66 reaches 100% and EL conversions on Ru/UiO-66–SO$_3$H and Ru/UiO-66–NO$_2$ increase to 72% and 27% which are ~24% and ~67% lower than those obtained by

employing 100 mg of the catalysts (95% for Ru/UiO-66–SO$_3$H and 82% for Ru/UiO-66–NO$_2$). The result indicates that the hydrogenation proceeds very fast in the presence of Ru/UiO-66 and the introduction of –NO$_2$ group hampers the hydrogenation of EL, while –SO$_3$H group plays a minor role in the hydrogenation of EL. With respect to transesterification of EHP, –SO$_3$H and –NO$_2$ groups play different roles in this step. The yields of GVL on Ru/UiO-66 for different dosages (25 mg, 50 mg and 100 mg) increase gradually from 39% to 45%, and to 50%, indicating a slow rate of transesterification of EHP. In the case of Ru/UiO-66–NO$_2$, a slight increase was found in the yield of GVL on 50 mg of Ru/UiO-66–NO$_2$ (53%) compared to the yield of GVL on 25 mg of Ru/UiO-66–NO$_2$ (50%), but a decreased yield of GVL (40%) was obtained by further increasing the amount of Ru/UiO-66–NO$_2$ to 100 mg, revealing that the introduction of –NO$_2$ group not only impedes the hydrogenation of EL but also the transesterification of EHP. It is noted that the yield of GVL on Ru/UiO-66–SO$_3$H increases significantly on increasing the dosage of Ru/UiO-66–SO$_3$H. The yield of GVL on 25 mg of Ru/UiO-66–SO$_3$H is 28% which is ~28% lower than the yield found on 25 mg of UiO-66. When the amount of Ru/UiO-66–SO$_3$H is increased to 50 mg, the yield of GVL increases to 52%, which is ~16% higher than that on 50 mg of Ru/UiO-66 and ~86% higher than that obtained on 25 mg of Ru/UiO-66–SO$_3$H. Further employing 100 mg of Ru/UiO-66–SO$_3$H, the yield of GVL is increased by ~118% compared to the yield of GVL when using 25 mg of Ru/UiO-66–SO$_3$H and is 22% higher than that obtained on 100 mg of Ru/UiO-66. The remarkable improvement indicates a faster transesterification of EHP and a positive role of –SO$_3$H group in the transesterification of EHP catalyzed by Ru/UiO-66, which may be attributed to the Brønsted acidity of –SO$_3$H.

4 Conclusions

In summary, the catalytic activity of Ru nanoparticles supported on Zr-UiO-66 and its analogues with various functional groups (–NO$_2$, –SO$_3$H and –NH$_2$) for hydrogenation of EL was systematically studied. The introduction of functional groups –NH$_2$ and –NO$_2$ reduces the activity of UiO-66 in both the hydrogenation of EL and the transesterification of EHP. The poor activity of Ru/UiO-66–NH$_2$ can be explained by the absence of metallic Ru particles, which is because of the strong coordination between Ru and –NH$_2$ groups. The Lewis acidity of –NO$_2$ results in the reduced activity of Ru/UiO-66 in the hydrogenation of EL. In contrast, –SO$_3$H group plays a positive role in the transesterification of EHP, resulting in an increase of 22% in the yield of GVL, in spite of a slightly reduced activity (EL conversion: 100% for Ru/UiO-66 vs. 95% for Ru/UiO-66–SO$_3$H). Reaction kinetics study further suggests that the introduction of –SO$_3$H group is beneficial for the transesterification of EHP due to its Brønsted acidity.

Conflicts of interest

There are no conflicts to declare.

Table 3 Catalytic performance of Ru/UiO-66 and Ru/UiO-66–X for EL hydrogenation in water[a]

Catalyst	Catalyst loading (mg)	Conv. (%)	Sel. (%)	
			GVL	EHP
Ru/UiO-66	100	100	50	50
	50	100	45	55
	25	98	39	61
Ru/UiO-66–SO$_3$H	100	95	61	39
	50	72	52	48
	25	29	28	72
Ru/UiO-66–NH$_2$	100	37	29	71
Ru/UiO-66–NO$_2$	100	82	40	60
	50	27	53	47
	25	11	50	50

[a] Reaction conditions: EL (0.34 mL), solvent (9.6 mL), 80 °C, 1 h, H$_2$ (0.5 MPa).

Acknowledgements

References

1 M. He, Y. Sun and B. Han, *Angew. Chem., Int. Ed.*, 2013, **52**, 9620–9633.

2 P. Gallezot, *Chem. Soc. Rev.*, 2012, **41**, 1538–1558.

3 A. J. Ragauskas, C. K. Williams, B. H. Davison, G. Britovsek, J. Cairney, C. A. Eckert, W. J. Frederick, J. P. Hallett, D. J. Leak, C. L. Liotta, J. R. Mielenz, R. Murphy, R. Templer and T. Tschaplinski, *Science*, 2006, **311**, 484–489.

4 R. A. Sheldon, *Green Chem.*, 2014, **16**, 950–963.

5 C. O. Tuck, E. Pérez, I. T. Horváth, R. A. Sheldon and M. Poliakoff, *Science*, 2012, **337**, 695–699.

6 J. P. Lange, R. Price, P. M. Ayoub, J. Louis, L. Petrus, L. Clarke and H. Gosselink, *Angew. Chem., Int. Ed.*, 2010, **49**, 4479–4483.

7 A. Villa, M. Schiavoni, C. E. Chan-Thaw, P. F. Fulvio, R. T. Mayes, S. Dai, K. L. More, G. M. Veith and L. Prati, *ChemSusChem*, 2015, **8**, 2520–2528.

8 D. M. Alonso, S. G. Wettstein and J. A. Dumesic, *Green Chem.*, 2013, **15**, 584–595.

9 P. G. Jessop, *Green Chem.*, 2011, **13**, 1391–1398.

10 C. E. Chan-Thaw, M. Marelli, R. Psaro, N. Ravasio and F. Zaccheria, *RSC Adv.*, 2013, **3**, 1302–1306.

11 Z. Yan, L. Lin and S. Liu, *Energy Fuels*, 2009, **23**, 3853–3858.

12 E. I. Gurbuz, D. M. Alonso, J. Q. Bond and J. A. Dumesic, *ChemSusChem*, 2011, **4**, 357–361.

13 A. H. Valekar, K.-H. Cho, S. K. Chitale, D.-Y. Hong, G.-Y. Cha, U. H. Lee, D. W. Hwang, C. Serre, J.-S. Chang and Y. K. Hwang, *Green Chem.*, 2016, **18**, 4542–4552.

14 X. Tang, H. Chen, L. Hu, W. Hao, Y. Sun, X. Zeng, L. Lin and S. Liu, *Appl. Catal., B*, 2014, **147**, 827–834.

15 K. Yan and A. Chen, *Fuel*, 2014, **115**, 101–108.

16 A. S. Piskun, J. E. de Haan, E. Wilbers, H. H. van de Bovenkamp, Z. Tang and H. J. Heeres, *ACS Sustainable Chem. Eng.*, 2016, **4**, 2939–2950.

17 A. M. Hengne, N. S. Biradar and C. V. Rode, *Catal. Lett.*, 2012, **142**, 779–787.

18 F. Ye, D. Zhang, T. Xue, Y. Wang and Y. Guan, *Green Chem.*, 2014, **16**, 3951–3957.

19 P. P. Upare, J.-M. Lee, D. W. Hwang, S. B. Halligudi, Y. K. Hwang and J.-S. Chang, *J. Ind. Eng. Chem.*, 2011, **17**, 287–292.

20 S. G. Wettstein, J. Q. Bond, D. M. Alonso, H. N. Pham, A. K. Datye and J. A. Dumesic, *Appl. Catal., B*, 2012, **117–118**, 321–329.

21 M. L. Testa, L. Corbel-Demailly, V. La Parola, A. M. Venezia and C. Pinel, *Catal. Today*, 2015, **257**, 291–296.

22 K.-I. Shimizu, S. Kanno and K. Kon, *Green Chem.*, 2014, **16**, 3899–3903.

23 H. Zhou, J. Song, H. Fan, B. Zhang, Y. Yang, J. Hu, Q. Zhu and B. Han, *Green Chem.*, 2014, **16**, 3870–3875.

24 D. Sun, A. Ohkubo, K. Asami, T. Katori, Y. Yamada and S. Sato, *Mol. Catal.*, 2017, **437**, 105–113.

25 E. F. Mai, M. A. Machado, T. E. Davies, J. A. Lopez-Sanchez and V. Teixeira da Silva, *Green Chem.*, 2014, **16**, 4092–4097.

26 W. Luo, M. Sankar, A. M. Beale, Q. He, C. J. Kiely, P. C. Bruijnincx and B. M. Weckhuysen, *Nat. Commun.*, 2015, **6**, 6540–6549.

27 A. M. Ruppert, J. Grams, M. Jędrzejczyk, J. Matras-Michalska, N. Keller, K. Ostojska and P. Sautet, *ChemSusChem*, 2015, **8**, 1538–1547.

28 Y. Kuwahara, Y. Magatani and H. Yamashita, *Catal. Today*, 2015, **258**, 262–269.

29 Y. Wang, Z. Rong, Y. Wang, T. Wang, Q. Du, Y. Wang and J. Qu, *ACS Sustainable Chem. Eng.*, 2016, **5**, 1538–1548.

30 A. M. R. Galletti, C. Antonetti, V. De Luise and M. Martinelli, *Green Chem.*, 2012, **14**, 688–694.

31 S. Horike, S. Shimomura and S. Kitagawa, *Nat. Chem.*, 2009, **1**, 695–794.

32 G. Ferey, *Chem. Soc. Rev.*, 2008, **37**, 191–214.

33 Y. Kuwahara, H. Kango and H. Yamashita, *ACS Sustainable Chem. Eng.*, 2017, **5**, 1141–1152.

34 A. Corma, H. García and F. X. Llabrési Xamena, *Chem. Rev.*, 2010, **110**, 4606–4655.

35 L. Ma, C. Abney and W. Lin, *Chem. Soc. Rev.*, 2009, **38**, 1248–1256.

36 J. Lee, O. K. Farha, J. Roberts, K. A. Scheidt, S. T. Nguyen and J. T. Hupp, *Chem. Soc. Rev.*, 2009, **38**, 1450–1459.

37 J. B. DeCoste, M. H. Weston, P. E. Fuller, T. M. Tovar, G. W. Peterson, M. D. LeVan and O. K. Farha, *Angew. Chem., Int. Ed.*, 2014, **53**, 14092–14095.

38 M. Zhang, C. Chen, Q. Wang, W. Fu, K. Huang and W. J. Zhou, *J. Mater. Chem. A*, 2017, **5**, 349–354.

39 A. Chakraborty, A. Achari, M. Eswaramoorthy and T. K. Maji, *Chem. Commun.*, 2016, **52**, 11378–11381.

40 J. Fu, S. Das, G. Xing, T. Ben, V. Valtchev and S. Qiu, *J. Am. Chem. Soc.*, 2016, **138**, 7673–7680.

41 L. E. Kreno, K. Leong, O. K. Farha, M. Allendorf, R. P. Van Duyne and J. T. Hupp, *Chem. Rev.*, 2012, **112**, 1105–1125.

42 J. J. Gassensmith, J. Y. Kim, J. M. Holcroft, O. K. Farha, J. F. Stoddart, J. T. Hupp and N. C. Jeong, *J. Am. Chem. Soc.*, 2014, **136**, 8277–8282.

43 J. H. Cavka, S. Jakobsen, U. Olsbye, N. Guillou, C. Lamberti, S. Bordiga and K. P. Lillerud, *J. Am. Chem. Soc.*, 2008, **130**, 13850–13851.

44 Y. R. Lee, Y. M. Chung and W. S. Ahn, *RSC Adv.*, 2014, **4**, 23064–23067.

45 R. Ghorbani-Vaghei, D. A. Davood Azarifar, S. Daliran and A. R. Oveisi, *RSC Adv.*, 2016, **6**, 29182–29189.

46 U. S. F. Arrozi, H. W. Wijaya, A. Patah and Y. Permana, *Appl. Catal., A*, 2015, **506**, 77–84.

47 J. F. Blandez, A. Santiago-Portillo, S. Navalón, M. Giménez-Marqués, M. Álvaro, P. Horcajada and H. García, *J. Mol. Catal. A: Chem.*, 2016, **425**, 332–339.

48 Y. Guo, Y. Li, J. Chen and L. Chen, *Catal. Lett.*, 2016, **146**, 2041–2052.

49 Z. Zhang, J. Chen, Z. Bao, G. Chang, H. Xing and Q. Ren, *RSC Adv.*, 2015, **5**, 79355–79360.

50 T. L. Doan, T. Q. Dao, H. N. Tran, P. H. Tran and T. N. Le, *Dalton Trans.*, 2016, **45**, 7875–7880.

51 N. E. Thornburg, Y. Liu, P. Li, J. T. Hupp, O. K. Farha and J. M. Notestein, *Catal. Sci. Technol.*, 2016, **6**, 6480–6484.

52 B. Van de Voorde, I. Stassen, B. Bueken, F. Vermoortele, D. De Vos, R. Ameloot, J. –C. Tan and T. D. Bennett, *J. Mater. Chem. A*, 2015, **3**, 1737–1742.

53 M. J. Katz, Z. J. Brown, Y. J. Colon, P. W. Siu, K. A. Scheidt, R. Q. Snurr, J. T. Hupp and O. K. Farha, *Chem. Commun.*, 2013, **49**, 9449–9451.

54 F. Vermoortele, M. Vandichel, B. Van de Voorde, R. Ameloot, M. Waroquier, V. Van Speybroeck and D. E. De Vos, *Angew. Chem., Int. Ed.*, 2012, **51**, 4887–4890.

55 R. C. Klet, Y. Liu, T. C. Wang, J. T. Hupp and O. K. Farha, *J. Mater. Chem. A*, 2016, **4**, 1479–1485.

56 M. Lin Foo, S. Horike, T. Fukushima, Y. Hijikata, Y. Kubota, M. Takata and S. Kitagawa, *Dalton Trans.*, 2012, **41**, 13791–13794.

57 M. Kandiah, M. H. Nilsen, S. Usseglio, S. Jakobsen, U. Olsbye, M. Tilset, C. Larabi, E. A. Quadrelli, F. Bonino and K. P. Lillerud, *Chem. Mater.*, 2010, **22**, 6632–6640.

58 J. Hou, Y. Luan, J. Tang, A. M. Wensley, M. Yang and Y. Lu, *J. Mol. Catal. A: Chem.*, 2015, **407**, 53–59.

59 Q. Yuan, D. Zhang, L. V. Haandel, F. Ye, T. Xue, E. J. M. Hensen and Y. Guan, *J. Mol. Catal. A: Chem.*, 2015, **406**, 58–64.

60 D. J. Morgan, *Surf. Interface Anal.*, 2015, **47**, 1072–1079.

61 S. Wang, Z. Zhang, B. Liu and J. Li, *Ind. Eng. Chem. Res.*, 2014, **53**, 5820–5827.